Equivalent Reactance of a Shorting Septum in a Fin-Line: Theory and Experiment

JEFFREY B. KNORR, MEMBER, IEEE

Abstract—**This paper presents the results of theoretical and experimental investigations of the equivalent reactance of a shorting septum in a fin-line. Numerical and experimental data showing septum reactance for several different fin-lines are presented and compared. Some design curves are included for millimeter-wave fin-lines with this type of discontinuity.**

I. Introduction

THE USE of fin-line as a millimeter-wave circuit medium has been discussed rather widely in the microwave literature during the past several years. Various fin-line components and circuits have been described and a number of analyses have been published. The analytical work which has been presented thus far has dealt with methods for determining the wavelength and characteristic impedance of a fin-line. While this is very necessary, it alone is not sufficient to permit the practical application of fin-line in millimeter-wave circuits. It is also necessary to analyze the various types of discontinuities that are required in order to realize the impedances needed in a practical circuit of finite extent.

One fin-line discontinuity which is of practical interest is the shorting septum. Located in the plane of the fins, the ideal, lossless septum is a perfectly reflecting termination which may be produced conveniently by printed circuit methods. Fig. 1 shows a fin-line cavity with a shorting septum at each end. A large current flows on the septum, and behind a reference plane coincident with the end of the septum the net stored energy is magnetic. (It is assumed here that the fin-line is operated in the dominant mode at a frequency below the cutoff for the next highest order mode.) The septum is not an ideal short, therefore, but behaves like a perfectly reflecting inductive reactance at the specified reference plane. The equivalent circuit for the cavity of Fig. 1 is shown in Fig. 2. It is a transmission line terminated with an inductor which represents the reactance of the septum as seen at the reference plane.

Theoretically, the equivalent reactance of the septum may be found by first determining the fin-line wavelength, λ', at a given frequency and then determining the shortest resonant length of the structure at that same frequency. The reactance is then found from the difference between the resonant length and $\lambda'/2$. Experimentally, the equivalent reactance may be measured using a suitably constructed test fixture with which a perfect short may be established at the desired reference plane. By measuring the difference between the angle of the reflection coefficient of the septum and that of the perfect short the reactance may be determined.

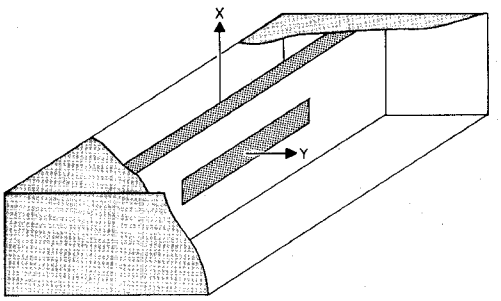

Fig. 1. Cutaway view of a fin-line cavity with a shorting septum at each end.

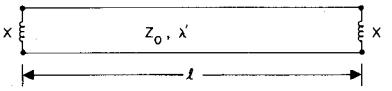

Fig. 2. Equivalent circuit representation of a fin-line with a shorting septum.

The purpose of this paper is to present the results of an investigation of the equivalent reactance of a septum in a fin-line. The septum was investigated both theoretically and experimentally. Section II describes the theoretical and experimental methods employed in the investigation and Section III presents the numerical and experimental data. Section IV contains some useful millimeter-wave fin-line circuit design data.

II. Theoretical and Experimental Methods

A. Theoretical Method

The theoretical analysis of the fin-line resonator may be carried out using the spectral domain method which has been discussed in several earlier papers by the author and co-workers [1]–[3]. A microstrip resonator has also been analyzed by Itoh using this method [4]. It will be shown below that the analysis of the fin-line resonator may be carried out by making relatively minor modifications to the equations developed for fin-line transmission [3]. The fields in the fin-line cavity may be written in the form [5]

$$E_{zi} = \left(\frac{\partial^2}{\partial z^2} + k^2 \right) \phi_i^e \tag{1a}$$

Manuscript received February 23, 1981; revised July 13, 1981. This work was supported by the Naval Postgraduate School Foundation Research Program.

The author is with the Department of Electrical Engineering, Naval Postgraduate School, Monterey, CA 93940.

0018-9480/81/1100-1196$00.75 ©1981 IEEE

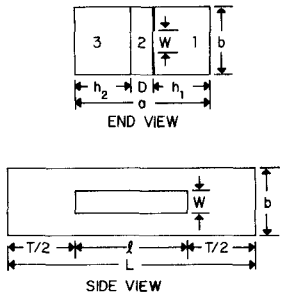

Fig. 3. End and side views of fin-line cavity showing dimensions and regions.

$$H_{zi}=\left(\frac{\partial}{\partial z^2}+k^2\right)\phi_i^h \tag{1b}$$

$$E_{xi}=\frac{\partial^2\phi_i^e}{\partial x\partial z}-j\omega\mu_i\frac{\partial\phi_i^h}{\partial y} \tag{1c}$$

$$E_{yi}=\frac{\partial^2\phi_i^e}{\partial y\partial z}+j\omega\mu_i\frac{\partial\phi_i^h}{\partial x} \tag{1d}$$

$$H_{xi}=j\omega\epsilon_i\frac{\partial\phi_i^e}{\partial y}+\frac{\partial^2\phi_i^h}{\partial x\partial z} \tag{1e}$$

$$H_{yi}=-j\omega\epsilon_i\frac{\partial\phi_i^e}{\partial x}+\frac{\partial^2\phi_i^h}{\partial y\partial z} \tag{1f}$$

where the scalar potential functions $\phi_i^e(x, y, z), \phi_i^h(x, y, z)$ satisfy the Helmholtz equation

$$\nabla^2\phi_i+k_i^2\phi_i=0 \tag{2}$$

and

$$k_i^2=\omega^2\mu_i\epsilon_i$$

for each of the three regions $i=1,2,3$ as shown in Fig. 3. For this problem we define the two-dimensional Fourier transform

$$\Phi_i(\alpha_n, y, \xi_k)=\int_{-L/2}^{+L/2}\int_{-b/2}^{+b/2}\phi_i(x, y, z)e^{j\alpha_n x}e^{j\xi_k z}\,dz\,dx \tag{3}$$

where

$$\alpha_n=\begin{cases}2n\dfrac{\pi}{b}, & \phi^h \text{ even in } x \quad (4a)\\ (2n-1)\dfrac{\pi}{b}, & \phi^h \text{ odd in } x \quad (4b)\end{cases}$$

$$\kappa_k=\begin{cases}2k\dfrac{\pi}{L}, & \phi^h \text{ odd in } z \quad (5a)\\ (2k-1)\dfrac{\pi}{L}, & \phi^h \text{ even in } z. \quad (5b)\end{cases}$$

With this definition the Helmholtz equation is transformed to obtain

$$\frac{\partial^2\Phi_i}{\partial y^2}(\alpha_n, y, \xi_k)=\gamma_i^2\Phi(\alpha_n, y, \xi_k) \tag{6}$$

with

$$\gamma_i^2=\alpha_n^2-\left(k_i^2-\xi_k^2\right). \tag{7}$$

Next, the solutions for the Φ_i are obtained. Equation (6) and boundary conditions are applied to obtain the set of transformed boundary equations. When these equations are compared with those for fin-line transmission [3], it is found they are identical if we choose

$$\xi_i=-\beta \tag{8}$$

where

$$\beta=\frac{2\pi}{\lambda'} \tag{9}$$

is the propagation constant which appears in the fin-line transmission analysis. Thus the final form of the equations,

$$\mathcal{G}_{11}(\alpha_n, \xi_k, \lambda)\mathcal{E}_x(\alpha_n, \xi_k)+\mathcal{G}_{12}(\alpha_n, \xi_k, \lambda)\mathcal{E}_z(\alpha_n, \xi_k)=\mathcal{J}_x(\alpha_n, \xi_k) \tag{10a}$$

$$\mathcal{G}_{21}(\alpha_n, \xi_k, \lambda)\mathcal{E}_x(\alpha_n, \xi_k)+\mathcal{G}_{22}(\alpha_n, \xi_k, \lambda)\mathcal{E}_z(\alpha_n, \xi_k)=\mathcal{J}_z(\alpha_n, \xi_k) \tag{10b}$$

is exactly the same as for fin-line transmission. The $\mathcal{G}_{pq}$ are the Fourier transformed components of the dyadic Green's function, $\mathcal{E}_x$ and $\mathcal{E}_z$ are the transformed components of the electric field in the plane of the fins at $y=D$ and $\mathcal{J}_x$ and $\mathcal{J}_z$ are the transformed components of the surface current on the fins.

Equations (10) may be further manipulated to eliminate $\mathcal{J}_x$ and $\mathcal{J}_z$ through the application of Galerkin's Method. Define the inner product as

$$\langle A(\alpha_n, \xi_k), B(\alpha_n, \xi_k)\rangle=\sum_{n=-\infty}^{+\infty}\sum_{k=-\infty}^{+\infty}A(\alpha_n, \xi_k)B^*(\alpha_n, \xi_k). \tag{11}$$

Then taking the inner product of (10a) with $\mathcal{E}_x$ and (10b) with $\mathcal{E}_z$ and applying Parseval's theorem, we obtain

$$\langle\mathcal{G}_{11}\mathcal{E}_x, \mathcal{E}_x\rangle+\langle\mathcal{G}_{12}\mathcal{E}_z, \mathcal{E}_x\rangle=0 \tag{12a}$$

$$\langle\mathcal{G}_{21}\mathcal{E}_x, \mathcal{E}_z\rangle+\langle\mathcal{G}_{22}\mathcal{E}_z, \mathcal{E}_z\rangle=0 \tag{12b}$$

where the right-hand side of (12) is zero because the current on the fins is orthogonal to the field between the fins. Explicit expressions for the $\mathcal{G}_{pq}$ exist and the field components $\mathcal{E}_x$ and $\mathcal{E}_z$ may be expanded in a suitable set of basis functions. The resonant frequency of the cavity is then found from (12) by numerical computation. It is interesting to note that the fin geometry enters the problem only through $\mathcal{E}_x$ and $\mathcal{E}_z$.

The accuracy of the solution obtained using (12) depends upon the quality of the basis set used to expand $\mathcal{E}_x$ and $\mathcal{E}_z$. In practice, the accuracy must be traded off against computation time, memory space and program complexity. Previous work has shown that accurate results may be obtained under the assumption $\mathcal{E}_z\approx 0$ in which case (12a) simplifies to

$$\sum_n\sum_k\mathcal{G}_{11}(\alpha_n, \xi_k, \lambda)|\mathcal{E}_x(\alpha_n, \xi_k, W, b, l, L)|^2=0.$$

It is also known from previous work that accurate results are obtained when the field between the fins is assumed constant with respect to x. The main problem in the present case is thus to expand $\mathcal{E}_x$ in such a manner that the amplitude variation of the x directed electric field (between the fins) with respect to z is properly represented.

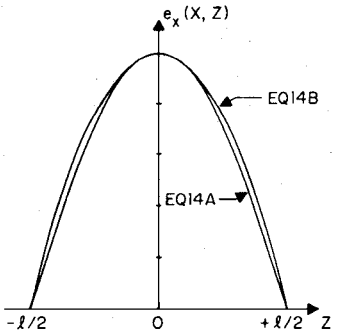

Fig. 4. One term approximations to e_x for the case $l=0.4\lambda'$.

Two different single-term expansions of $\mathcal{E}_x$ were investigated. These were obtained from Fourier transformation of assumed electric field distributions, $e_x(x, z)$ between the fins given by

$$e_x(x, z)=A\cos\left(\frac{\pi z}{l}\right), \qquad |x|\leq W/2,\ |z|\leq l/2 \quad (14a)$$

and

$$e_x(x, z)=A\cos\left(\frac{2\pi z}{\lambda'}\right)-A\left[\frac{\cos\frac{\pi l}{\lambda'}}{\cosh\frac{Cl}{2}}\right]\cosh\left(\frac{Cl}{2}\frac{2z}{l}\right), \qquad |x|\leq W/2,\ |z|\leq l/2 \quad (14b)$$

where in (14b) C is a parameter which will be discussed. Both 14(a) and 14(b) assume the field is independent of x. Equation 14(a) assumes a sinusoidal variation of field with z with the amplitude going to zero at $z=\pm l/2$. This is exactly correct for the case where the septum is absent ($T=0$). However, as the septum protrudes further into the cavity and the equivalent reactance terminating the cavity increases, the correctness of this representation deteriorates. This deterioration was reflected in poor accuracy of the numerical results obtained using (14a). The representation of (14b) corrects this difficulty. The first term of (14b) gives the correct amplitude variation for the dominant mode. When the cavity is reactively terminated, $l<\lambda'/2$, this term is nonzero for $z=\pm l/2$. The total field, e_x, is zero, however, due to the presence of evanescent modes. The presence of the evanescent modes is accounted for approximately by the second term of (14b). The rate of decay is adjusted by the parameter $Cl/2$. The results obtained using (14b) appeared to be quite satisfactory and were not extremely sensitive to the choice of $Cl/2$. The value $Cl/2=10$ was used in the computations reported here. The basis function of (14b) will be referred to as the end corrected basis function. The basis functions of (14) are plotted in Fig. 4 for the case $l=0.4\lambda'$ which corresponds to an equivalent normalized septum reactance, $x=0.158$.

The theoretical method described above provides a straightforward procedure for calculating the equivalent reactance of a fin-line septum. For a specified frequency and structure geometry the first step is to calculate the fin-line wavelength, λ', [3]. Next, the shortest resonant length, l, is calculated for the same frequency and geometry. The difference between the length of a perfectly shorted

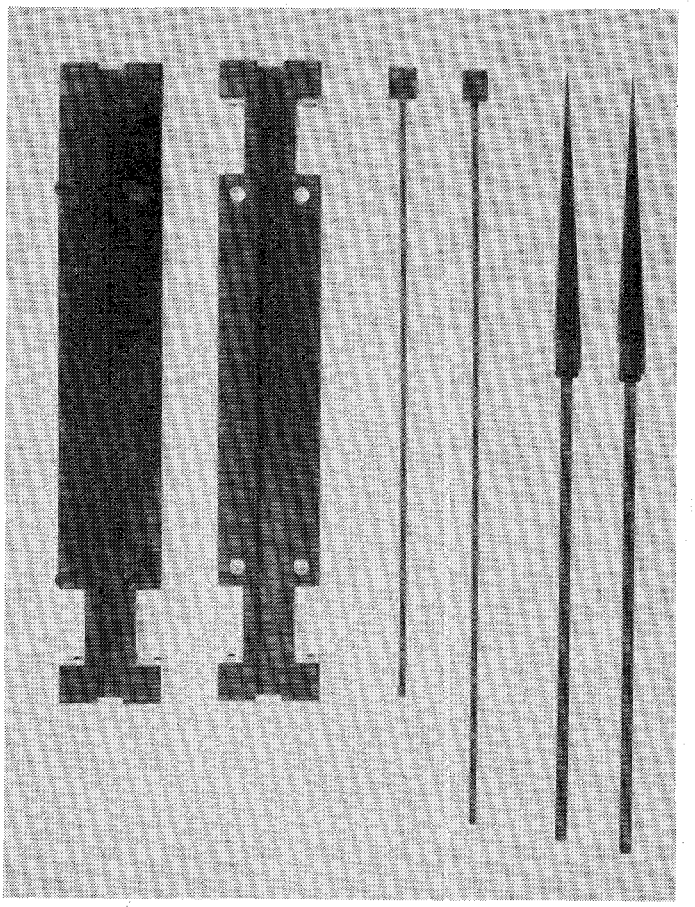

Fig. 5. Photograph of waveguide test fixture, a fin, shorting blocks, and wedge terminations.

cavity and the length of a reactively terminated cavity is

$$2\Delta l=(\lambda'/2)-l \quad (15)$$

which may be used to calculate the equivalent reactance

$$x=\tan(2\pi\Delta l/\lambda'). \quad (16)$$

This relation holds for any septum length, $T/2$. The equivalent reactance of a long septum is found simply by allowing $T/2$ to become large which effectively eliminates interaction between the fields and the end wall of the cavity.

B. Experimental Method

Experimental measurements of septum reactance were made using a test fixture which was machined specifically for that purpose. The measurements were carried out in the 8–12-GHz frequency range for reasons related to availability of test instrumentation and ease of fabrication of the test fixture. The test fixture consisted of a 10-in length of X-band guide ($a=0.9$ in, $b=0.4$ in) machined in two identical longitudinal sections which were bolted together. The necessary fin patterns were etched from 0.002-in thick beryllium copper sheet and inserted between the two halves of the shielding guide. No dielectric material was present. Shorting blocks and wedge terminations were constructed in such a manner that they could be positioned on both sides of the fin. A photograph of all the test apparatus is shown in Fig. 5.

The experimental measurements reported here were all obtained with $\epsilon_{r2}=1$ (no dielectric) as described above. The decision not to print the fins on dielectric was made because in practice the dielectric must be positioned and secured in the shield. This is done by machining a groove or a slot in the wall of the shield. In this case the actual fin-line geometry differs from that shown in Fig. 3 and this introduces a source of measurement uncertainty that is difficult to quantify. Thus the use of fins but no dielectric resulted, we believe, in the closest possible correspondence between the experimental structure and its theoretical model.

Measurements were made on fin-lines with $W/b=0.1$, $W/b=0.5$, and $W/b=1.0$. When $W/b=1.0$, we have a special case, that of a bifurcated guide. In this case the septum is preceeded by empty, unloaded rectangular waveguide and it is convenient to measure the reactance of the septum by observing the standing wave pattern with a slotted line. It is a simple procedure to place a short at the end of the slotted line to establish the load position and then to replace the short with the test fixture. A metal septum is placed in the test fixture and the leading edge of the septum is aligned with the flange on the test fixture so that it is in the same plane as was the short. This method was employed here for $W/b=1.0$ and is believed to yield experimental results with uncertainty limited to several percent.

For the fin-lines with $W/b<1$, the septum was printed at one end of the fin-line while at the other end was printed a tapered transition to the empty waveguide from which the fin-line was excited. The test fixture was connected to a HP 8410S microwave network analyzer through a slide screw tuner and precision waveguide to coax transition. For each measurement frequency, sliding matched terminations were first placed along the finned section of line and the slide screw tuner was used to eliminate reflections. The sliding terminations were then removed and replaced by the shorting blocks which were aligned with the end of the septum to establish the reference plane for calibration of the network analyzer. The shorting blocks were then removed and the normalized reactance of the septum was measured.

Although considerable care was taken to obtain accurate experimental data, it was not possible to eliminate all sources of experimental error. The two most significant sources of error appear to be due to positioning and to matching as discussed below:

1) Positioning Error: The reference plane is established by positioning sliding shorting blocks to the plane coincident with the leading edge of the septum. This must be accomplished after the fixture is assembled with the fins in place and some phase error may result from imprecise positioning. The phase error $\Delta\phi$ due to a positioning error Δl is given by

$$\Delta\phi/\Delta l=720/\lambda' \text{ degrees/m} \tag{17}$$

where λ' is the fin-line wavelength. Suppose, for example, $\lambda'=30$ mm, a typical value for the X-band lines used in this study. Then the error is 24°/mm. If it is assumed the shorting blocks can be positioned with an accuracy of $\pm.1$ mm, then the phase error is $\Delta\phi=\pm 2.4$ degrees. If the measured reactance is $x=0.190$ ($\Gamma=1\angle 159°$) the uncertainty in the reactance will be $\Delta x=\pm.023$ and the error is ± 12 percent. This clearly illustrates the fact that a very small positioning error will introduce a significant uncertainty in the measured reactance.

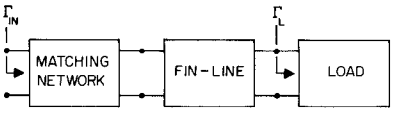

Fig. 6. Error model for the determination of phase uncertainty due to a matching network.

2) Matching Error: For network analyzer measurements the analyzer was connected to the fin-line with its septum through a coax-waveguide transition, slide screw tuner and tapered transition. The slide screw tuner was adjusted to obtain the best possible match (smallest reflection) between the analyzer and the fin-line when the sliding matched terminations were in place along the fin-line just ahead of the septum. The combination of transition-tuner-taper may be modeled as a two-port network through which the reflection from the septum must be viewed. This is illustrated in Fig. 6.

The reflection coefficient, Γ_{in}, measured at the input to the matching network is

$$\Gamma_{in}=S_{11}+\Gamma_L' \tag{18}$$

where

$$\Gamma_L'=\frac{S_{12}S_{21}\Gamma_L}{1-S_{22}\Gamma_L} \tag{19}$$

is the load reflection coefficient, Γ_L, transferred to the input of the matching network. If the matching network is assumed lossless and reciprocal with $|S_{11}|=|S_{22}|<0.1$ the difference between the angle of Γ_L and the angle of Γ_L' can be shown to be

$$\phi_L'-\phi_L=2\phi_{12}+|S_{11}|\sin(\phi_{22}+\phi_L). \tag{20}$$

The matching network, therefore, introduces a phase uncertainty, $\Delta\phi\leqslant\pm|S_{11}|$ radians when either the reference short or the septum is measured. In the worst case the total error would be less than $2|S_{11}|$ if the errors for short and septum add together. Thus the phase uncertainty introduced by the matching network is bounded by

$$\Delta\phi\leqslant\pm 2|S_{11}| \text{ rad.} \tag{21}$$

When the fin-line is terminated in a perfect matched load, $\Gamma_L=0$ and the reflection coefficient seen at the input of the matching network is $\Gamma_{in}=S_{11}$. The matching procedure described here typically resulted in $|\Gamma_{in}|\approx 0.01$. Assuming a perfect load, the corresponding phase uncertainty due to the matching network was therefore ± 1.1 degrees. If the matched load is not perfect then there will be some instances where the phase error due to matching will be greater.

The uncertainty due to matching error must be added to the uncertainty due to positioning. For the conditions cited

in the example discussed under positioning error it was shown that an uncertainty of ± 12 percent resulted from a positioning error of ± 0.1 mm. If we assume the phase error due to matching is ± 1.1 degrees (which is probably optimistic) then the total phase uncertainty in this example is ± 3.5 deg and the resultant error in reactance may be as large as ± 17 percent.

Clearly, although the measurement of septum reactance is straightforward in principle, it is not an easy task to achieve high experimental accuracy in practice. This is particularly true when $W/b<1$ and the problem becomes more serious as W/b is made smaller because the fin-line wavelength, λ', decreases.

III. Numerical and Experimental Results

The numerical data obtained using the theoretical method described in Section II of this paper have been compared with other available theoretical results and with experimental data. For those cases where such comparisons were made, the various results were found to agree quite well as described below.

A. Comparison with Other Theory

When $W/b=1$ and $\epsilon_i=\epsilon_0$ for all three fin-line regions, we obtain the special case of a bifurcated rectangular waveguide when T is large. Results for this special case have been presented by Marcuvitz [6]. Fig. 7 shows the normalized septum reactance versus frequency for a bifurcated X-band waveguide. The dashed curves were computed using the spectral-domain method with (14a) and the solid curves were computed using the end corrected basis function of (14b). The discrete points (x) were plotted using data from [6]. Clearly, there is good agreement between the two theories when the basis function of (14b) is used. There is considerable disagreement when (14a) is used. The experimental results were also in close agreement when (14b) was used and it was, therefore, concluded that the quality of this approximation was good.

B. Comparison with Experiment

Measurements of septum reactance were made in X-band using fin-lines with $W/b=1.0$, $W/b=0.5$, and $W/b=0.1$. In all cases the fins were centered ($h_1=a/2$) and no dielectric was present ($\epsilon_i=\epsilon_o$ for all three regions).

Fig. 8 shows the normalized reactance calculated using (14b) (solid curves) and the measured reactance (discrete points). The experimental data for $W/b=1$ were obtained from slotted line measurements and the uncertainty is believed to be small. The difference between the calculated and measured reactance values is better than 5 percent in all cases. The experimental data for $W/b=0.5$ and $W/b=0.1$ were obtained using a network analyzer. This required the use of transitions and a more complex tuning and calibration procedure as described earlier. The errors which resulted introduced a greater experimental uncertainty than in the case $W/b=1$. This is seen in Fig. 8 where the discrepancy between numerical and experimental results is somewhat greater for $W/b=0.5$ and $W/b=0.1$.

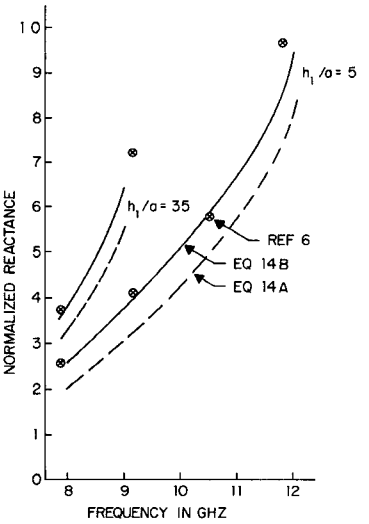

Fig. 7. Normalized septum reactance versus frequency for a bifurcated WR (90) X-band waveguide with the septum in several different positions $\epsilon_{r2}=1$, $T\to\infty$.

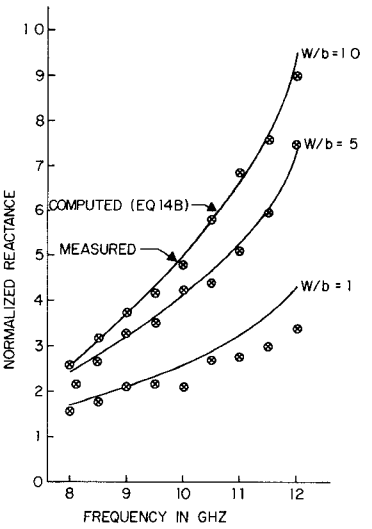

Fig. 8. Normalized septum reactance versus frequency for several fin-lines. Fins are centered and shield is WR (90) X-band guide $\epsilon_{r2}=1$, $T\to\infty$.

Several effects cause the difference between theory and experiment to increase as W/b decreases. First, at a given frequency the fin-line wavelength, λ', decreases as W/b becomes smaller. This causes the phase uncertainty associated with positioning error to increase. Second, as W/b decreases the fin-line field becomes more concentrated in the region of the fins which causes the termination to behave less ideally. Finally, although the fin thickness was only 0.002 in, the effect of the finite metal thickness was unknown. It is to be expected, however, that any error due to fin thickness will increase with decreasing W/b since the field becomes more concentrated in the vicinity of the fins. This deduction follows from perturbation theory.

C. Effect of Septum Length

The effect of septum length was investigated numerically by calculating the septum reactance for various values of

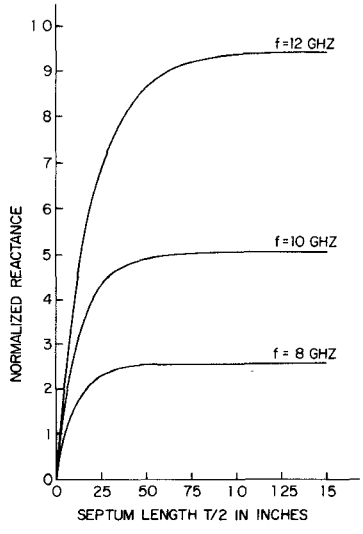

Fig. 9. Normalized septum reactance versus septum length for several frequencies. Fins are centered, $W/b=1$, $\epsilon_{r2}=1$ and shield is *WR* (90) *X*-band guide.

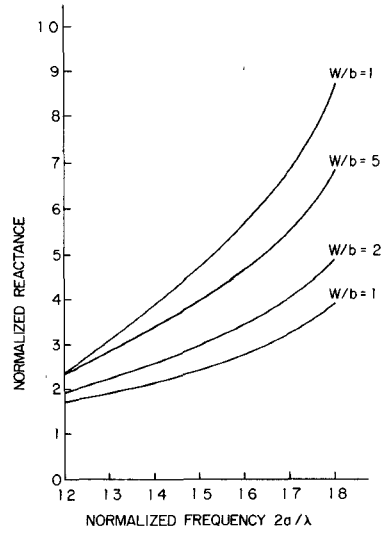

Fig. 10. Normalized septum reactance versus normalized frequency for a fin-line with $\epsilon_{r2}=2.2$, $b/a=0.5$, $h_1/a=0.5$, $D/a=0$, and $T\rightarrow\infty$.

distance from the leading edge of the septum to the end of the cavity. This is shown in Fig. 9. For all frequencies, the reactance increases rapidly as the length of the septum is increased and then saturates. Once the distance to the end wall of the cavity has become sufficiently large there is negligible interaction between the field and the end wall. Beyond this point the reactance does not change with further increases in septum length. It can also be seen from Fig. 9 that the septum length required to reach maximum reactance increases with frequency. This is a result of the fact that the evanescent field behind the leading edge of the septum decays more slowly as the frequency increases.

Some experimental measurements were made to verify the computed curves shown in Fig. 9. The results were quite satisfactory. These data are not shown here, however, since the test fixture was not designed in such a way that highly accurate results could be obtained.

IV. Design Curves

The structure which has been discussed here is described by a number of independently variable parameters. This precludes the possibility of producing any finite set of universal design curves. However, in practice fin-lines are normally constructed with the fins at or near the center of the shield because of bandwidth considerations. Further, if dielectric is used, it is normally thin (typically, $D=0.005$ in) and one popular choice of material has $\epsilon_r=2.2$. Thus the design curves shown in Figs. 10–12 should prove useful in many cases of practical interest. These curves cover the frequency range over which the empty shield would normally be operated in the TE_{10} waveguide mode.

An inspection of the curves in Figs. 10–12 shows that the reactance tends to increase as the thickness of the dielectric increases. The increase in reactance results from a relatively higher proportion of stored magnetic energy beyond the leading edge of the septum. This in turn is caused by a slower decay of the field on the dielectric loaded side of the septum. It is not universally true that the dielectric

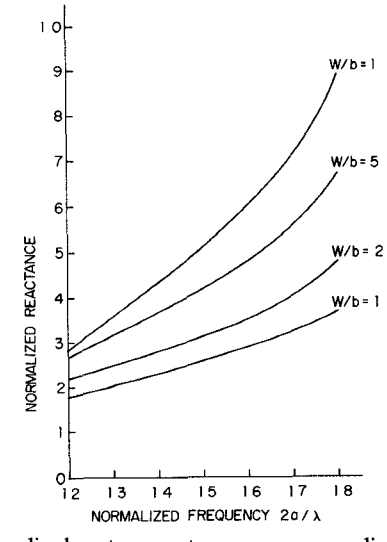

Fig. 11. Normalized septum reactance versus normalized frequency for a fin-line with $\epsilon_{r2}=2.2$, $b/a=0.5$, $h_1/a=0.5$, $D/a=0.05$, and $T\rightarrow\infty$.

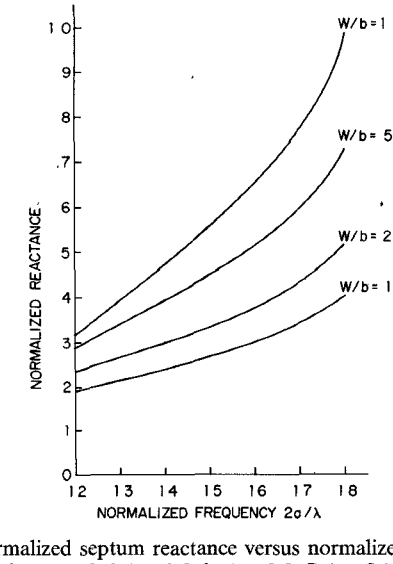

Fig. 12. Normalized septum reactance versus normalized frequency for a fin-line with $\epsilon_{r2}=2.2$, $b/a=0.5$, $h_1/a=0.5$, $D/a=0.10$, and $T\rightarrow\infty$.

will cause an increase in reactance, however. For $2\ a/\lambda = 1.8$, for example, the reactance first decreases slightly and then increases as the dielectric thickness is increased from $D/a = 0$ to $D/a = 0.1$.

V. Conclusions

The application of the spectral domain method to the analysis of a fin-line resonator has been described. It has been shown the equivalent reactance of a bifurcating septum may be found by this method. Numerical and experimental data for septum reactance have been presented and have been shown to be in quite good agreement. Since the fin-line wavelength, λ', is used in the calculation of the septum reactance, the results presented here also provide an indirect verification of the accuracy of the wavelength calculations described in [3]. Selected design curves have been presented which should cover many cases encountered in practice.

The successful use of the spectral-domain approach in solving the septum discontinuity problem treated here suggests that the method should prove useful in solving a variety of planar line discontinuity problems.

Acknowledgment

The author wishes to acknowlege the contribution of LT. Guy Miller, U.S. Navy who supervised the design of the experimental apparatus and provided some of the experimental data reported here.

References

[1] J. B. Knorr and K-D. Kuchler, "Analysis of coupled slots and coplanar strips on dielectric substrate," *IEEE Trans. Microwave Theory Tech.*, vol. MTT-23, pp. 541–548, July 1975.

[2] J. B. Knorr and A. Tufekcioglu, "Spectral-domain calculation of microstrip characteristics impedance," *IEEE Trans. Microwave Theory Tech.*, vol. MTT-23, pp. 725–728, Sept. 1975.

[3] J. B. Knorr and P. M. Shayda, "Millimeter-wave fin-line characteristics," *IEEE Trans. Microwave Theory Tech.*, vol. MTT-28, pp. 737–743, July 1980.

[4] T. Itoh, "Analysis of microstrip resonators," *IEEE Trans. Microwave Theory Tech.*, vol. MTT-22, pp. 946–962, Nov. 1974.

[5] R. Harrington, *Time Harmonic Electromagnetic Fields*. New York: McGraw-Hill, 1961.

[6] N. Marcuvitz, *Waveguide Handbook*. New York: McGraw-Hill, 1951.

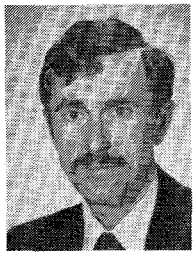

Jeffrey B. Knorr (S'68–M'71) was born in Lincoln Park, NJ, on May 8, 1940. He received the B.S. and M.S. degrees in electrical engineering from Pennsylvania State University, University Park, in 1963 and 1964, respectively, and the Ph.D. degree in electrical engineering from Cornell University, Ithaca, NY, in 1970.

From 1964 to 1967 he served with the U.S. Navy. In September 1970, he joined the faculty of the Naval Postgraduate School, Monterey, CA, where he currently holds the rank of Associate Professor in the Department of Electrical Engineering. He is also a member of the interdisciplinary Electronic Warfare Academic Group which is responsible for the administration of the Electronic Warfare Curriculum at the Naval Postgraduate School.

Dr. Knorr is a member of Sigma Xi.

Energy Absorption from Small Radiating Coaxial Probes in Lossy Media

MAYS L. SWICORD SENIOR MEMBER, IEEE, AND CHRISTOPHER C. DAVIS

***Abstract*—This paper describes the calculation of energy deposition around small open-ended coaxial antenna probes in lossy media. Two theoretical methods, a small monopole approximation (I) and an equivalent magnetic current source (II), are evaluated and compared. Method I is shown to be inappropriate for determining near field energy deposition. Power contour plots determined by method II in the vicinity of the open-ended coaxial antenna are presented as well as calculations of total power absorbed as a function of distance from the antenna center for various antenna dimensions and media dielectric properties. Our calculations of absorbed power distributions near the antenna are consistent with the limited experimental data which is available for comparison. A frequency of 2.45 GHz was selected for these calculations so that the results will be of value to workers interested in the application of open-ended coaxial antennas for invasive treatment of cancer by microwave hyperthermia.**

Manuscript received March 6, 1981; revised June 29, 1981.

M. L. Swicord is with the Bureau of Radiological Health, Rockville, MD 20857.

C. C. Davis is with the Electrical Engineering Department, University of Maryland, College Park, MD 20742.

I. Introduction

CALCULATIONS of field distributions and energy deposition around small open-ended coaxial probes in lossy media have been made and are reported here. Such small probes have been used or proposed for use in dielectrometry, hyperthermic treatment of small tumors and microwave spectroscopic investigations of liquids. The results of this investigation are instructive in all of the above cases, but will, it is hoped, be particularly helpful to those

0018-9480/81/1100-1202$00.75 ©1981 IEEE